Electronic Supplementary Material (ESI) for CrystEngComm.

<Electronic Supplementary Information>

Interfacial effects of crystal surface through free quinolinyl groups on crystal organization and catalysis

Byung Joo Kim, Haeri Lee, Tae Hwan Noh and Ok-Sang Jung*

Department of Chemistry, Pusan National University, Pusan 609-735, Korea

Table S1 Crystal refinement parameters for $[CuCl_2L]_2$, $[CuBr_2L]_2$, $[HgCl_2L]_2$, and $[HgBr_2L]_2$

	$[CuCl_2L]_2$	$[CuBr_2L]_2$	$[HgCl_2L]_2$	$[HgBr_2L]_2$
Formula	1/2 $C_{72}H_{42}Cl_4Cu_2N_6O_{12}$	1/2 $C_{72}H_{42}Br_4Cu_2N_6O_{12}$	1/2 $C_{72}H_{42}Cl_4Hg_2N_6O_{12}$	1/2 $C_{72}H_{42}Br_4Hg_2N_6O_{12}$
M_w	726.00	814.92	863.05	951.97
Crystal system	Orthorhombic	Orthorhombic	Orthorhombic	Orthorhombic
Space group	*Cmca*	*Cmca*	*Cmca*	*Cmca*
a [Å]	26.648(3)	26.8621(2)	26.7895(7)	26.8929(9)
b [Å]	14.3871(1)	14.5732(8)	14.5479(4)	14.6597(4)
c [Å]	15.1191(1)	15.1408(7)	15.1124(5)	15.0879(4)
V [Å^3]	5796.6(8)	5927.1(6)	5889.8(3)	5948.3(3)
Z	8	8	8	8
ρ [g cm^{-3}]	1.664	1.826	1.947	2.126
μ [mm^{-1}]	0.996	3.491	5.465	7.919
F(000)	2952	3240	3360	3648
Index ranges	$-32\le h\le 32$ $-17\le k\le 17$ $-18\le l\le 18$	$-33\le h\le 32$ $-17\le k\le 17$ $-18\le l\le 18$	$-33\le h\le 33$ $-18\le k\le 18$ $-18\le l\le 18$	$-33\le h\le 33$ $-18\le k\le 17$ $-18\le l\le 18$
Completeness	100.0% (θ = 25.99°)	100.0% (θ = 25.99°)	100.0% (θ = 26.49°)	100.0% (θ = 26.50°)
R_{int}	0.1597	0.1261	0.0531	0.0981
Goodness-of-fit	2.242	2.353	2.433	1.986
R_1 [$I>2\sigma(I)$][a]	0.2272	0.2047	0.1679	0.1384
wR_2 (all data)[b]	0.5743	0.5770	0.5272	0.4686

[a] $R_1 = \Sigma||F_o| - |F_c||/\Sigma|F_o|$, [b] $wR_2 = (\Sigma[w(F_o^2 - F_c^2)^2]/\Sigma[w(F_o^2)^2])^{1/2}$

Table S2 Selected bond lengths and [Å] and angles [°] for $[CuCl_2L]_2$, $[CuBr_2L]_2$, $[HgCl_2L]_2$, and $[HgBr_2L]_2$

$[CuCl_2L]_2$		$[CuBr_2L]_2$	
Cu(1)–N(1)	2.120(1)	Cu(1)–N(1)	2.117(2)
Cu(1)–N(1)$^{\#1}$	2.120(1)	Cu(1)–N(1)$^{\#3}$	2.117(2)
Cu(1)–Cl(1)	2.224(5)	Cu(1)–Br(1)	2.381(3)
Cu(1)–Cl(1)$^{\#1}$	2.224(5)	Cu(1)–Br(1)$^{\#3}$	2.381(3)
Cu(1)···Cu(1)$^{\#2}$	17.9791(2)	Cu(1)···Cu(1)$^{\#4}$	17.9807(1)
N(1)–Cu(1)–N(1)$^{\#1}$	151.5(7)	N(1)–Cu(1)–N(1)$^{\#3}$	155.3(1)
Cl(1)–Cu(1)–Cl(1)$^{\#1}$	151.7(3)	Br(1)–Cu(1)–Br(1)$^{\#3}$	147.2(2)
N(1)–Cu(1)–Cl(1)	95.0(3)	N(1)–Cu(1)–Br(1)	97.0(4)
N(1)–Cu(1)–Cl(1)$^{\#1}$	91.9(4)	N(1)$^{\#3}$–Cu(1)–Br(1)	89.9(5)
N(1)$^{\#1}$–Cu(1)–Cl(1)$^{\#1}$	95.0(4)	N(1)–Cu(1)–Br(1)$^{\#3}$	89.9(5)
$[HgCl_2L]_2$		$[HgBr_2L]_2$	
Hg(1)–N(1)	2.529(1)	Hg(1)–N(1)	2.531(1)
Hg(1)–N(1)$^{\#5}$	2.529(1)	Hg(1)–N(1)$^{\#7}$	2.531(1)
Hg(1)–Cl(1)	2.368(6)	Hg(1)–Br(1)	2.481(3)
Hg(1)–Cl(1)$^{\#5}$	2.368(6)	Hg(1)–Br(1)$^{\#7}$	2.481(3)
Hg(1)···Hg(1)$^{\#6}$	19.3120(5)	Hg(1)···Hg(1)$^{\#8}$	19.3374(6)
N(1)–Hg(1)–N(1)$^{\#5}$	128.7(7)	N(1)–Hg(1)–N(1)$^{\#7}$	125.4(6)
Cl(1)–Hg (1)–Cl(1)$^{\#5}$	167.9(3)	Br(1)–Hg(1)–Br(1)$^{\#7}$	166.26(2)
N(1)–Hg(1)–Cl(1)$^{\#5}$	90.8(3)	N(1)–Hg(1)–Br(1)	94.5(3)
N(1)$^{\#5}$– Hg(1)–Cl(1)	90.8(3)	N(1)$^{\#7}$–Hg(1)–Br(1)	91.8(3)
N(1)$^{\#5}$–Hg(1)–Cl(1)$^{\#5}$	94.5(3)	N(1)–Hg(1)–Br(1)$^{\#7}$	91.8(3)

$^{\#1}$x,–y,–z+2, $^{\#2}$2–x,–y,2–z, $^{\#3}$x,–y,–z+1, $^{\#4}$2–x,–y,1–z, $^{\#5}$x,–y+2,–z+1, $^{\#6}$2–x,2–y,1–z, $^{\#7}$x,–y+1,–z+2, $^{\#8}$2–x,1–y,2–z

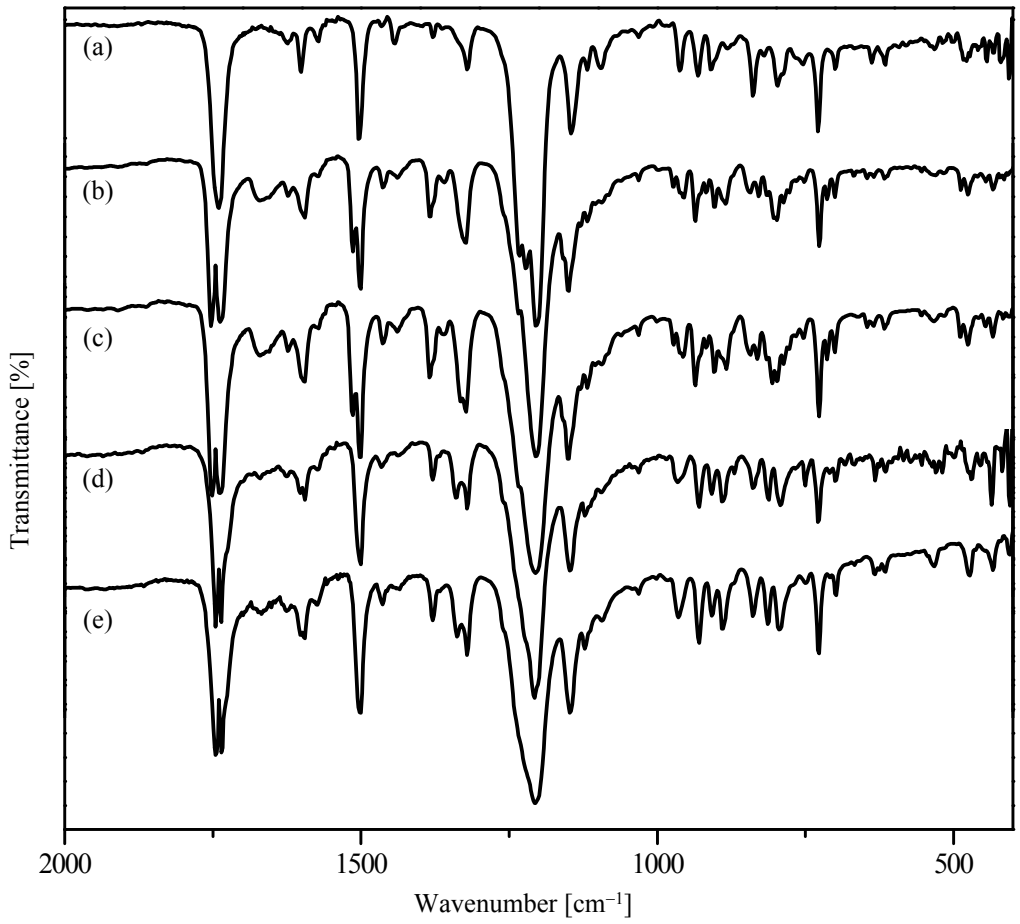

Fig. S1 IR spectra of L (a), $[CuCl_2L]_2$ (b), $[CuBr_2L]_2$ (c), $[HgCl_2L]_2$ (d), and $[HgBr_2L]_2$ (e).

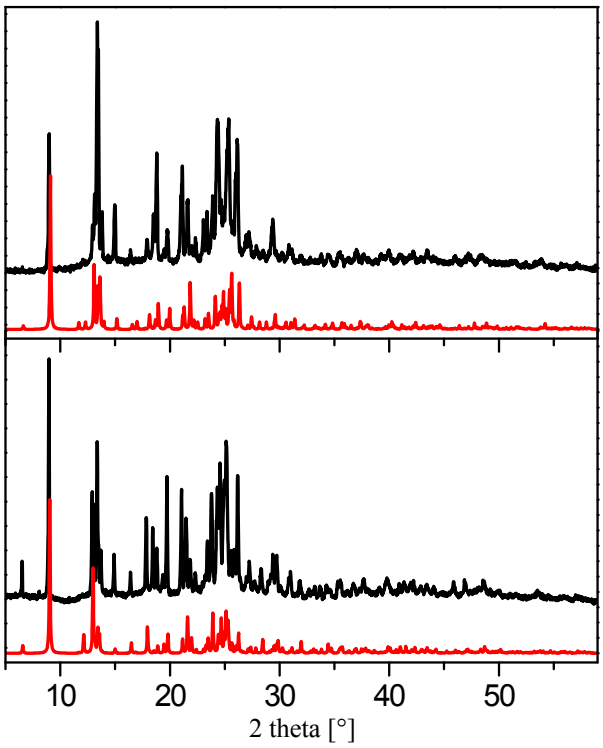

Fig. S2 Powder XRD patterns (black lines) for $[CuCl_2L]_2$ (a) and $[CuBr_2L]_2$ (b) along with the simulated pattern (red line) from single-crystal X-ray diffraction data.

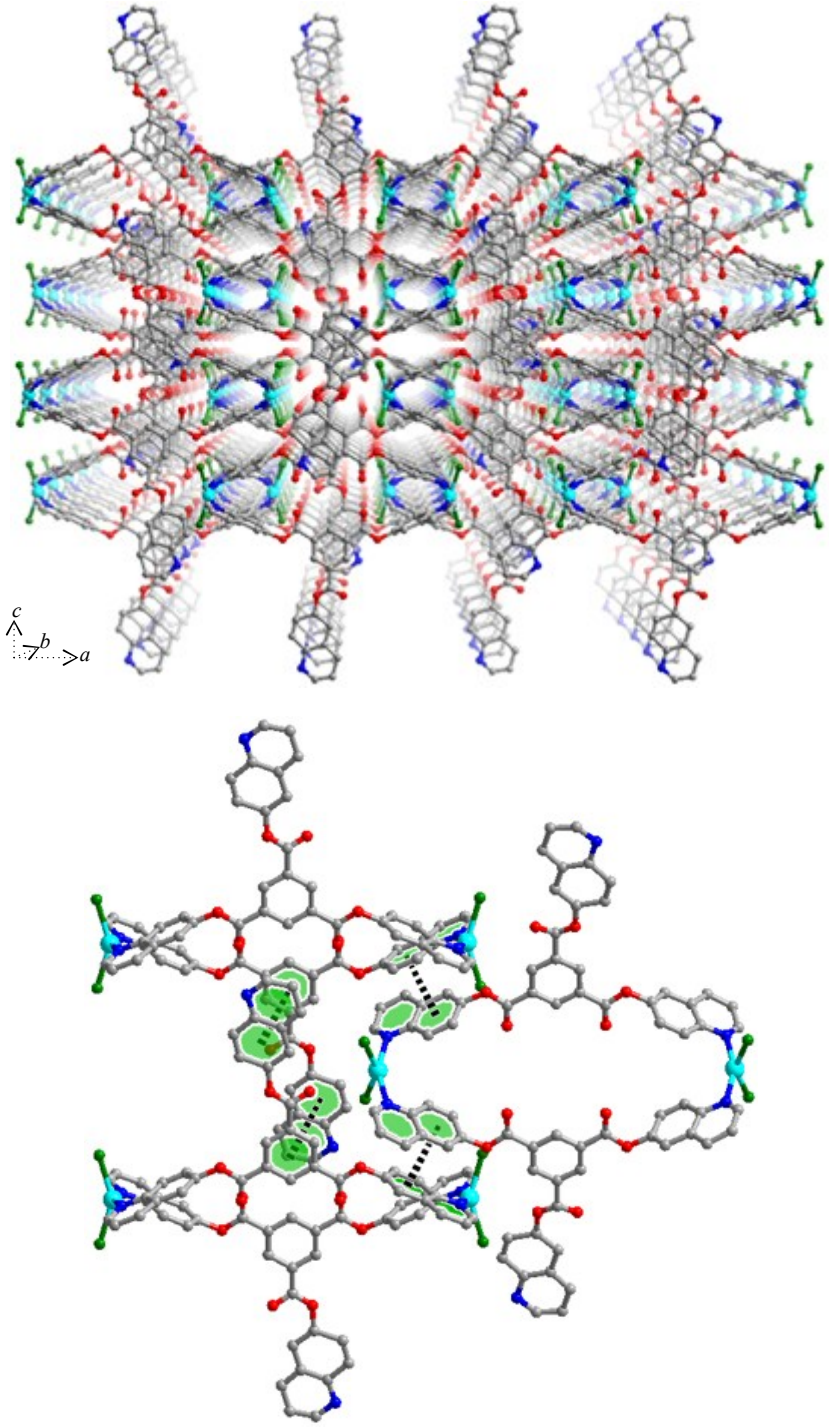

Fig. S3 Top: Crystal structure of $[CuCl_2L]_2$ showing packing diagram (top) and π···π interactions between the adjacent quinolinyl groups and between quinolinyl and central phenyl group in the solid state (bottom).

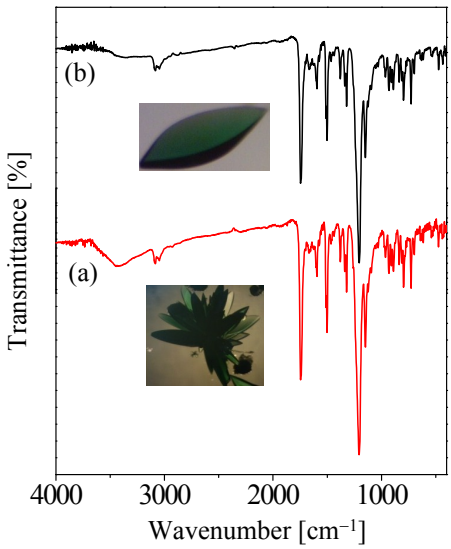

Fig. S4 IR spectra of $[CuCl_2L]_2$ aggregates (a) representing the existence of water molecules in contrast to single crystal (b).

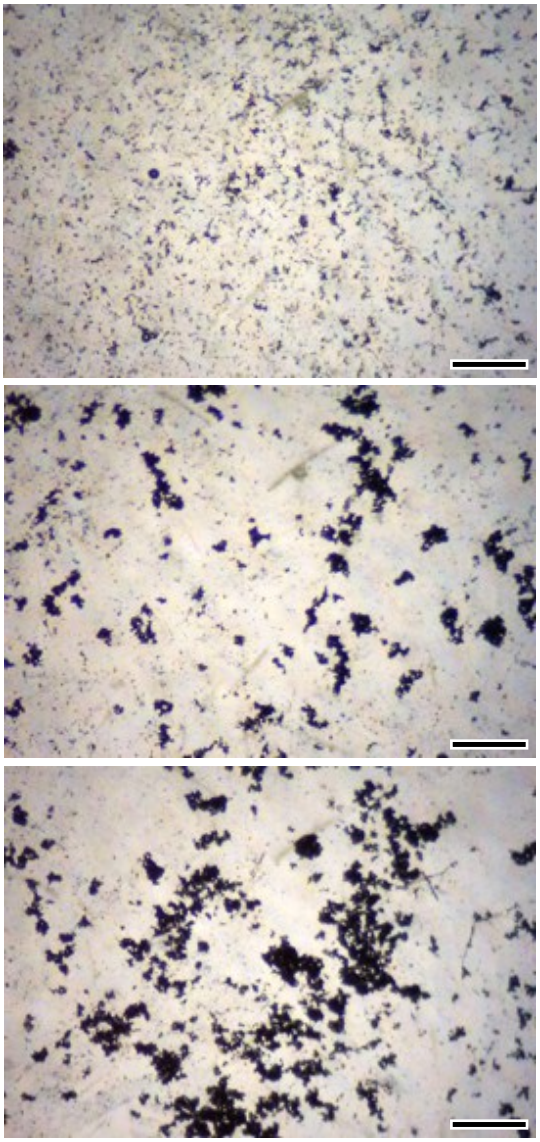

Fig. S5 Optical microscopic images showing self-aggregation of $[HgCl_2L]_2$ microcrystals in an aqueous solution: top, initial state; middle, after 12 h; bottom, after 1 day. Bar = 600 μm.

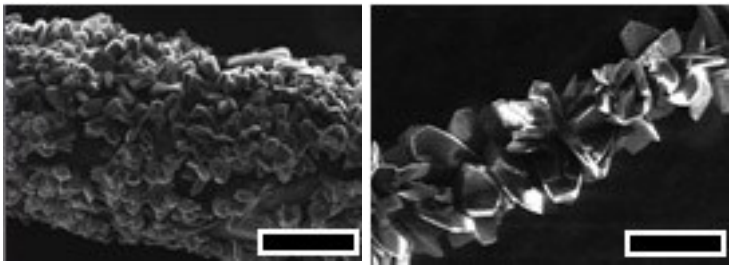

Fig. S6 SEM images of $[CuX_2L]_2$@cottom (left) and $[CuX_2L]_2$@glass (right) showing crystal growth in the presence of glass-fiber and cotton-thread, respectively.

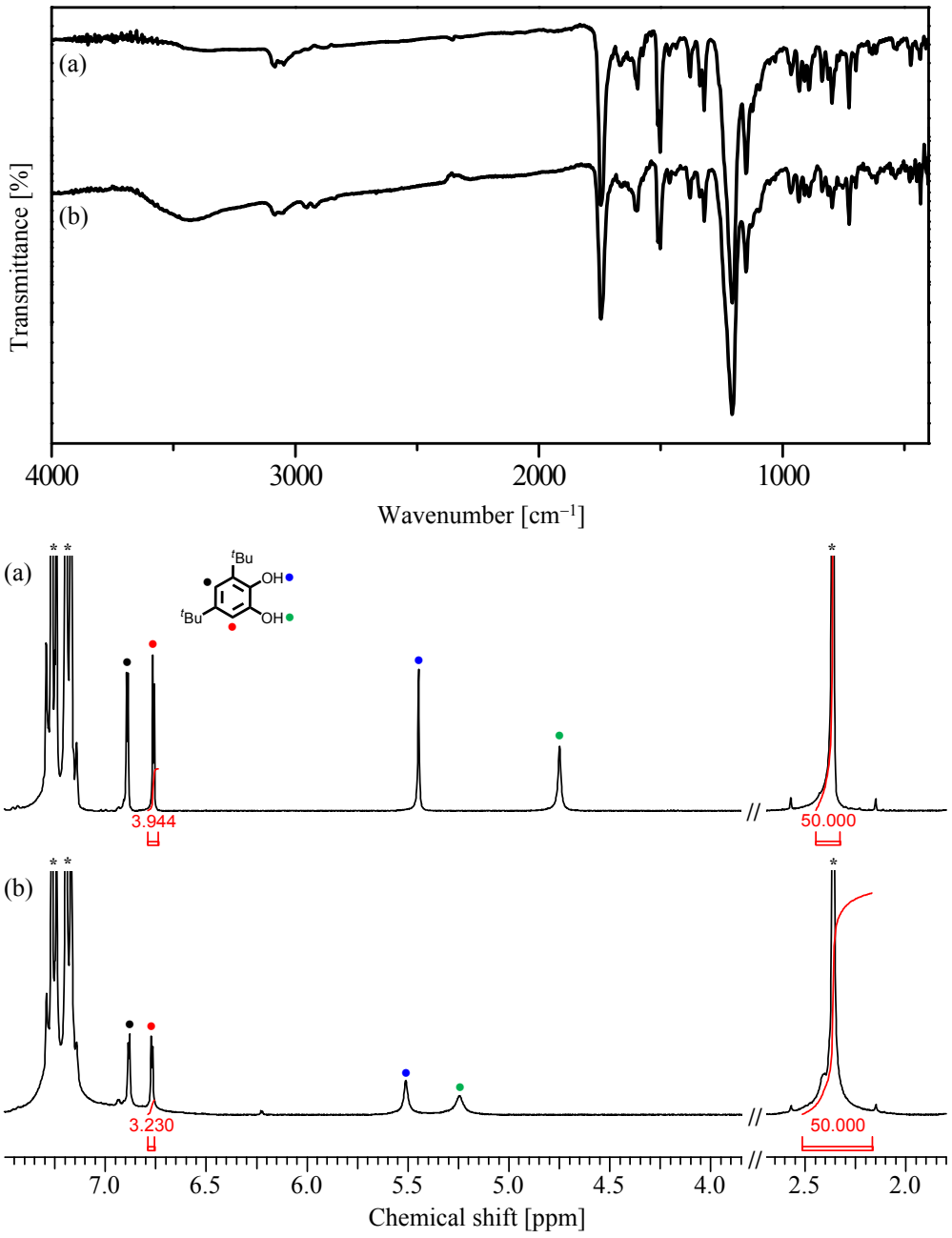

Fig. S7 Top: IR spectra of $[CuCl_2L]_2$ crystals before (a) and after (b) adsorption of 3,5-DBCat on the surface. 73 mg of $[CuCl_2L]_2$ crystals were immersed in a $CDCl_3$ solution of 3,5-DBCat at −15 °C for 6 h. Bottom: ^1H NMR spectra of the $CDCl_3$ solution before (a) and after (b) adsorption. Asterisks denote the resonances corresponding to toluene used as an internal reference.

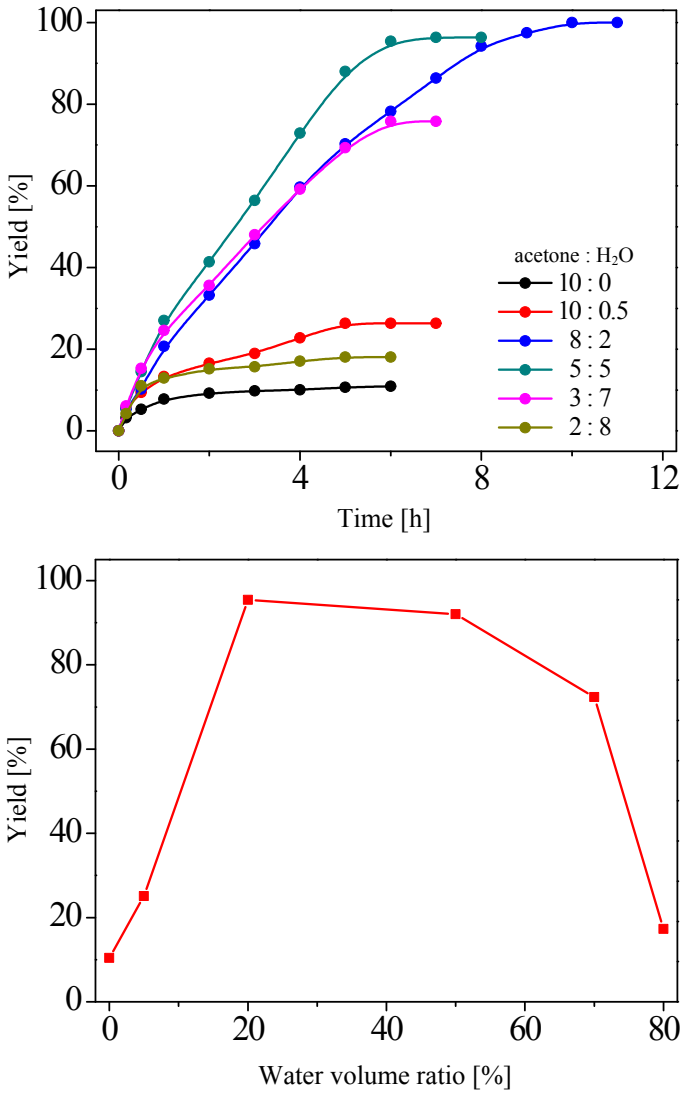

Fig. S8 Top: plot showing catalytic oxidation yields of 3,5-DBCat as a function of time using $[CuCl_2L]_2$ in a various mixture of acetone and water at 50 °C. Bottom: the final oxidation yield of 3,5-DBCat as a function of water volume ratio.

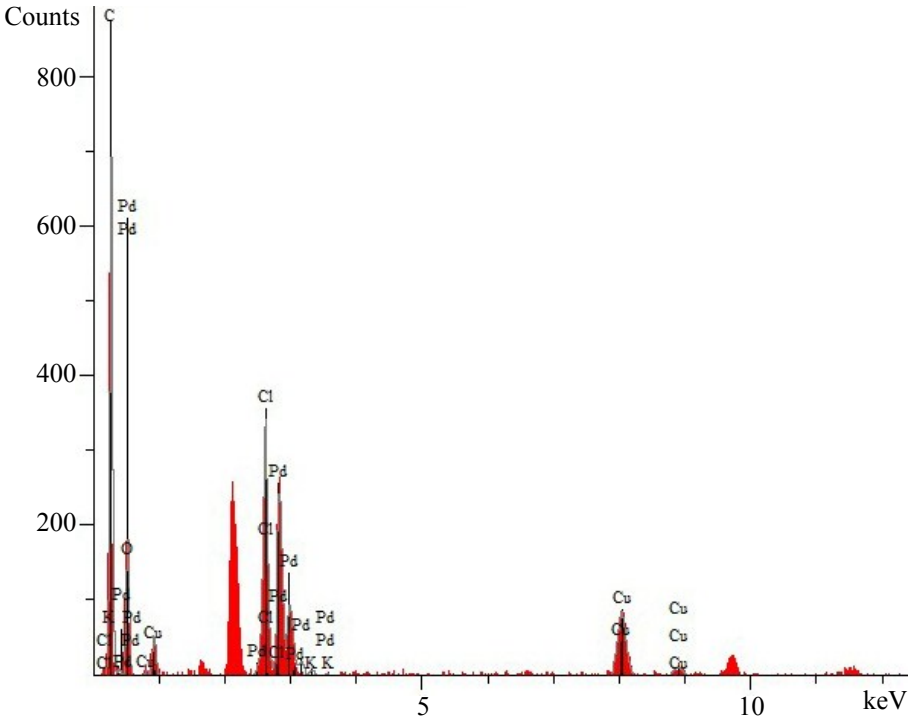

Fig. S9 SEM-EDX data for $PdCl_2$@$[CuCl_2L]_2$.